Chemical Engineering Journal 497 (2024) 154654

Contents lists available at ScienceDirect

Chemical Engineering Journal

journal homepage: www.elsevier.com/locate/cej

Valorization of olive mill waste fractions and production of furfural and 5-hydroxymethylfurfural by heterogeneous catalysis over Nb_2O_5, $NbOPO_4$ and TiO_2-PO_4 catalysts

Serena Lima [a], Tea Ricotta [a], Elisa I. García-López [b,*], Leonarda F. Liotta [c], Silvia Villar-Rodil [d], Gianluca Li Puma [a], Giuseppe Marcì [a], Francesca Scargiali [a]

[a] University of Palermo, Department of Engineering, Viale delle Scienze Ed. 6, 90128 Palermo, Italy
[b] University of Palermo, STEBICEF, Viale delle Scienze Ed. 16, 90128 Palermo, Italy
[c] Institute of Nanostructured Materials (ISMN)-CNR, via Ugo La Malfa, 153, 90146, Palermo, Italy
[d] Instituto de Ciencia y Tecnología del Carbono (INCAR-CSIC), C/Francisco Pintado Fe 26, 33011 Oviedo, Spain

ARTICLE INFO

Keywords:
Biomass catalytic conversion
Vegetation water
Olive pomace
Olive mill wastewater
Furans
Niobium based catalyst

ABSTRACT

The production of furans from the valorization of olive mill biomass waste streams including olive mill wastewater (OMW), olive virgin pomace (OVP), dry pelletized pomace (DPP), and olive dry leaves (DL) was investigated using acidic Nb_2O_5, $NbOPO_4$ and TiO_2-PO_4 heterogeneous catalysts. Batch reactions were performed in an autoclave at 210 °C in the presence of the suspended catalysts and the yield of furfural and 5-hydroxymethylfurfural (5-HMF) was determined. The valorization of OMW was found more effective in the presence of $NbOPO_4$ as a result of its high acidity nature. The amount and strength of the acid sites of $NbOPO_4$ were much higher than the other catalysts. The highest yield of hexoses sugars in OMW to 5-HMF was 44 %, while furfural was a minor product. The 5-HMF yield further increased to 91 % after pre-extraction of the polyphenolic species from the OMW. Recycling tests of $NbOPO_4$ catalyst, the most performant one, indicated the very good stability of this material. As result of the highest xylose content in the olive mill solids fractions (olive pomace, dry pellet pomace and dry leaves), furfural's yields of 100 %, 57 % and 31 %, respectively, were observed, while 5-HMF in contrast to OMW was a minor product. This work demonstrates the feasibility of using acidic catalysts for the valorization of olive mill waste streams targeting the desired furan product.

1. Introduction

The valorization of the biomass residues generated by a large range of agro-industrial activities is progressively becoming more influential to promote sustainable agriculture [1]. The production of olive oil is of fundamental importance to the economy of many Mediterranean countries which supply more than 90 % of the olive oil world production. Each 1000 kg of olives produce 980 kg of waste including 400 kg of olive pomace, i.e. the solid residue also known as olive press cake or olive virgin pomace (OVP) and 600 kg of aqueous olive mill wastewater (OMW) (Figure S1) [2]. Currently in many olive oil mills, the waste (OVP and OMW) is often discarded and treated as a costly hazardous waste, impacting the environment and resulting in an economic loss for the producers. However, OVP (including olive peel, kernel and water) contains a wide range of bioactive compounds, such as polyphenols, vitamins and minerals with significant economic value. For this reason, the efficient recovery of phenolic compounds [3] and the valorization of the carbohydrates residues through their conversion to high added value products [4] represent a significant opportunity to improve the sustainability of this agricultural sector. The OVP is mainly made of water, oil, olive peel, and kernels [5]. The dry residue, pelletised pomace (DPP), can be used as a fuel [6], and the dry pomace and leaves can be also used to prepare acid catalysts and/or as a source of valuable compounds [7]. The liquid waste OMW, however, is a highly hazardous waste fraction of major concern contributing to significant environmental contamination. OMW has a strong odor, and contains a high content of sugars, polyphenols (0.5–24 g/L), suspended solids (drupe residues) and a high organic load that is difficult to degrade [8]. The presence of phenolic compounds and organic acids confers to OMW phytotoxicity and antimicrobial properties leading to the inhibition of

* Corresponding author.
E-mail address: elisaisabel.garcialopez@unipa.it (E.I. García-López).

https://doi.org/10.1016/j.cej.2024.154654
Received 24 April 2024; Received in revised form 18 July 2024; Accepted 6 August 2024
Available online 8 August 2024

plant growth or even death. Consequently, a range of treatment methods have been investigated to remove the toxicity of OMW including biological aerobic and anaerobic processes, treatment with fungi or algae advanced oxidation technologies such as wet air oxidation, Fenton process, photocatalytic, ozonation, or electrochemical treatment, membrane technology, evaporation/drying and coagulation-flocculation [9].

The valorization of both OVP and OMW to produce high added value products is relatively under exploited in the olive oil industry. Indeed, molecules as glucose, xylose, and other monomeric sugars, present in olive waste fractions, can be exploited to yield high value products such as furans. Polymeric sugars in the waste can be extracted and hydrolyzed to simple sugars with chemical or physical treatment and further dehydrated to yield as main products furfural [10] and 5-hydroxymethyl-furfural (5-HMF) [11]. Furfural is a platform chemical for the synthesis of furfuryl alcohol, furoic acid, furan, tetrahydrofuran, 2-methyltetrahydrofuran, and related resins. 5-HMF is valuable [12] to produce dimethylfuran, used as fuel and solvent [13], furan dicarboxylic acid used for the production of polyesters [14] and gamma-valerolactone which is a platform molecule that can give adipic acid, a precursor of Nylon. Furans can also yield by condensation reaction insoluble humins and by hydration of 5-HMF also levulinic and formic acid. (Figure S2). The reactions reported in Figure S2 are normally carried in a homogeneous phase using mineral acids, even though solid catalyst could provide a more sustainable approach avoiding the further recovery of the catalyst and possible release to the environment. Although heterogeneous catalysis has been used for the treatment of waste streams from the olive oil industry [15,16] it has not been reported for the valorization to furans.

In this study, the production of furans from the valorization of olive mill biomass waste streams including olive mill wastewater (OMW), olive virgin pomace (OVP), dry pelletized pomace (DPP) (DPP), and olive dry leaves (DL) was investigated using acidic Nb_2O_5, $NbOPO_4$ and TiO_2-PO_4 heterogeneous catalysts. These abundant and non-toxic catalysts display both Brønsted (BAS) and Lewis acid sites (LAS) [17] (Figure S3) and these properties can be exploited to simultaneously isomerize glucose to fructose (LAS) and dehydrate fructose to 5-HMF (BAS). Valuable polyphenols were also recovered by extraction prior to catalytic treatment and a range of treatment methods were used to maximize the conversion of sugars to furans. Although the utilization of residuals from the olive industry for catalytic purposes has been documented, this study shows the potential of using a greener heterogenous catalytic process for the valorization of both liquid and solid waste fractions of the olive oil production process. This novel perspective holds significant potential for valorizing other waste agricultural waste materials in the context of a circular economy process.

2. Materials and methods

2.1. Olive mill waste streams

The olive mill waste streams (OMW, OVP, DPP and DL) were provided by Azienda Agricola D'Anna Francesca located in Castellammare del Golfo, in the region of Sicily, Italy which processes mixed olives of the cultivars Biancolilla, Nocellara and Cerasuola. The cultivars were collected in mid-October at the end of the maturation process. The polyphenols content of the OMW was recovered by liquid–liquid extraction using ethyl acetate as solvent. The extraction process was carried out at different temperatures (20, 40, 60 and 80 °C), both at the natural OMW pH (5.4–5.7) and at acidic pH (3.0). Briefly, 5 mL of the OMW solution and 50 mL of ethyl acetate were placed in a beaker, acidified with HCl if needed and magnetically stirred for 180 min. The ethyl acetate phase rich in polyphenols was collected, fully evaporated, redissolved in 5 mL of methanol and analyzed by HPLC, using a Q-Exactive LCq/Orbitrap MS instrumentation in HESI (Electrospray Ionization) in FULL SCAN MS negative ions mode. The analysis was performed at 30 °C with 400μL min^{-1} mobile phase flow, with the following composition: mobile phase A 0.1 % acetic acid, mobile phase B methanol; 0–2 min B 5 %, 2–5 min B 10 %, 5–16 min B 25 %, 16–30 min B 95 %, 30–35 min B 5 %. The separation column was a Luna C18(2) 150 x 2.0 mm, 5 μm stationary phase, equipped with a precolumn.

The total carbohydrate content of the OMW, OVP, DPP and DL was determined by the Dubois method with some adaptations [18]. 10 mg of each dry solid waste (OVP, DPP or DL) were firstly dissolved in 5 mL of 2 M HCl and maintained at 120 °C for 3 h to hydrolyze the polymeric complex sugars present in the samples. Then, 1 mL of the above solution or 1 mL of OMW, were supplemented with 1 mL of aqueous phenol solution (5 % ww), 1 mL of water, and 5 mL of concentrated H_2SO_4. After 20 min reaction time, the absorbance of the solution was measured at 490 nm and the concentration of total sugars was determined by a calibration curve. The sugars monomers were determined by HPLC analysis after enzymatic hydrolysis. Briefly, 1 mL of OMW or 20 mg of solid samples were mixed to 10 mL of water at pH 5.5 containing 25 μL of enzymes (Viscozyme, Novozyme). The enzymatic hydrolysis was kept at 45 °C for 3 h. Then the sample was filtered with 0.45 μm membrane filter (CA, Millipore) and injected into an Agilent 1220 HPLC equipped with a column Shodex SUGAR SP0810 and a RID 1260 detector. The eluent was ultrapure water at 600μL min^{-1}, the column temperature was 65 °C and the RID temperature 55 °C.

The OVP solid waste was initially freeze-dried for two days in a benchtop freeze-dryer (FreeZone 2.5 L, LABCONCO, USA) and further used or pre-treated in planetary ball mill (Retsch Grind Jars Comfort Ss 125 ML 014620148w/Free S&H, provided with a stainless-steel jar and 20 balls steel grinding balls for CyroMill, diameter: 10 mm) to facilitate the hydrolysis reaction. DPP was used as received or pre-treated in the

Table 1
Content of total sugars in OMW before and after the separation of polyphenols, and in OVP, in DPP and in DL. The conditions of the separation of polyphenols are reported in terms of temperature and pH of the solution in the extractive process.

Sample	Treatment condition	Total sugar content
Olive mill wastewater	–	11.7 ± 0.31 g•L^{-1}
Olive mill wastewater after polyphenol extraction	25 °C; natural pH	11.7 ± 0.31 g•L^{-1}
	25 °C; pH 3	12.0 ± 0.32 g•L^{-1}
	40 °C; pH 3	12.8 ± 0.35 g•L^{-1}
	60 °C; pH 3	11.8 ± 0.32 g•L^{-1}
	80 °C; pH 3	11.6 ± 0.31 g•L^{-1}
	40 °C; natural pH	11.6 ± 0.31 g•L^{-1}
	60 °C; natural pH	13.0 ± 0.35 g•L^{-1}
	80 °C; natural pH	11.5 ± 0.31 g•L^{-1}
Olive Virgin Pomace	–	42.3 ± 1.14 %
Dry Pellet Pomace	–	31.5 ± 0.85 %
Dry Leaves	–	66.0 ± 1.78 %

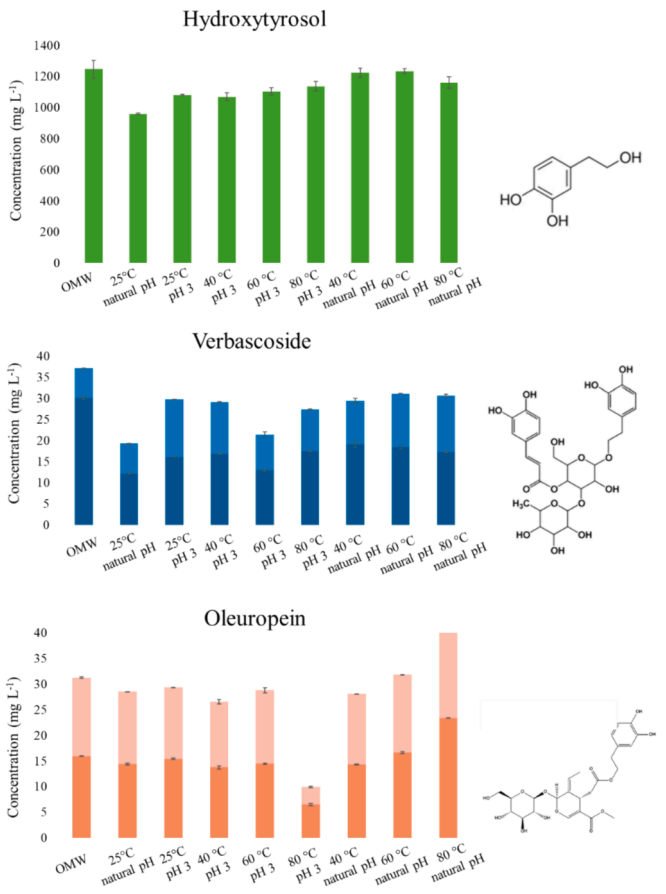

Fig. 1. Concentration of (A) hydroxytyrosol; (B) verbascoside; and (C) oleuropein, measured both in the original aqueous phase of the OMW and in the methanol solution after their extraction with ethyl acetate at different temperatures and pHs. For verbascoside and oleuropein two isomers have been analyzed, indicated with different colors in the figure.

planetary ball mill as above. DL were dried in an oven overnight at 60 °C before further treatment in the planetary ball mill. The ball-milling pretreatment was applied to 1 g of OVP, 1 g of DDP and to 500 mg of DL. The conditions were 30 or 10 min milling at 500 or 300 rpm. After the above pretreatment procedures, the samples were employed for the catalytic process as described in section 2.3.

2.2. Heterogeneous catalysts preparation and characterization

Nb_2O_5 amorphous hydrated oxide (purity 99.5 %) labelled as Nb_2O_5, and hydrated niobium oxyphospate $NbOPO_4$ (purity 99.4 %) were provided from the Companhia Brasileira de Metalurgia e Mineração (CBMM) and they were used as received. The Nb:P molar ratio in the $NbOPO_4$ was 1:0.44 [19]. The phosphated titanium oxide catalyst (TiO_2-PO_4) was synthesized in house by the sol–gel method. In detail, 4.4 g of pluronic P123 were dissolved in 50 g of anhydrous ethanol and stirred at room temperature for 1 h to obtain a transparent solution. Then, 11.2 g of titanium butoxide (99 % wt) and 1.1 g of HNO_3 (65 % wt) were added dropwise to the P123 solution immersed in an ice bath and stirred for 1 h. In another beaker, 0.2 g of H_3PO_4 (85 % wt) was dissolved in 3.3 g of anhydrous ethanol and 3.3 g of water, and the formed solution was added dropwise under vigorous stirring to the solution containing Ti. The Ti:P molar ratio was 1: 0.05. The resulting solution was further stirred in the ice bath for another hour and aged for 24 h at room temperature. The formed gel was dried at 60 °C in a static oven for 24 h and eventually calcined at 400 °C for 6 h with a heating rate of 2 °C•min^{-1} obtaining the solid labelled as TiO_2-PO_4 catalyst. All the materials were bulk and surface physical–chemical characterized. The specific surface areas (SSA), pore volume and pore size of the materials were determined from N_2 adsorption–desorption isotherms using a Micromeritics ASAP2020 system. Before analysis, the samples were degassed under vacuum at 100 °C for 12 h. Scanning electron microscopy (SEM) combined with energy dispersive X-ray spectroscopy (EDX) was carried out using a FEI Quanta 200 ESEM microscope, operating at 20 kV on specimens upon which a thin layer of gold had been evaporated. XPS analysis was performed on a SPECS spectrometer equipped with a Phoibos 100 hemispherical electron energy analyzer. The spectra were acquired at pressures below 10^{-7} Pa using a monochromatic Al Ka X-ray source operated at a voltage of 14.00 KV and a power of 175 W. The photo-excited electrons were analyzed in constant pass energy mode, using 50 for the survey and 10 eV for the high-resolution core level spectra, respectively. Spectra were recorded at a take-off angle of 90°. The specimens for XPS were prepared by sticking the powdered materials onto the XPS sample holder. The oxides and oxide mixtures are non-conductive and thus a positive charge builds on their surface as electrons are photoemitted from it, which shifts the XPS spectra to higher binding energies (BE). The charge effect was counterbalanced in situ with an electron flood gun. BE were referenced to the main C 1 s peak at 285.0 eV. CasaXPS software was used for data processing. The compositions in atomic percent (at. %) were determined from the survey spectra by considering the integrated peak areas of the main XPS peaks of the different elements and their respective sensitivity factors after corrections for the mean free-path of the outgoing electrons and the transmission function of the analyzer.

FTIR and Raman, were used to verify the structural features of the solids. FTIR spectra of the samples in KBr (Aldrich) pellets were obtained by using a FTIR-8400 Shimadzu spectrometer with 4 cm^{-1} resolution and 256 scans and spectra were recorded before and after the reaction to evidence the possible presence of humins. Raman spectra were registered by using a Renishaw in-via Raman spectrometer equipped with an integrated microscope and with a charged-coupled device (CCD) camera. A He/Ne laser operating at 632.8 nm was used as the exciting source. The power of the laser used was 15 % of the maximum value that was around 300 mW. The quantification of Brønsted acid sites on the surface of the materials was performed in aqueous suspension by the titration method [20]. In a typical experiment, 0.1 g of solid was added to 25 mL of deionized water and the resulting suspension was allowed to equilibrate for 24 h under continuous stirring, hence, it was titrated by dropwise addition of 0.01 M aqueous solution of NaOH using phenolphthalein as the neutralization indicator. On the other hand, the strength of the acid sites (both Brønsted and Lewis) of the catalysts was studied by Temperature Programmed Desorption of ammonia (NH_3-TPD) using a Micromeritics Autochem 2950 instrument equipped with an ultraviolet gas analyser (ABB, Limas 11). A preliminary study to test

Table 2
Specific surface area and acid properties of the used catalysts.

Catalyst	Specific surface area [$m^2 \cdot g^{-1}$]	Acid sites by NaOH titration [mmol $H^+ g^{-1}$]	Surface density of Brønsted acid sites [µmol $H^+ m^{-2}$]	Acid sites by NH_3-TPD [mmol $NH_3 \cdot g^{-1}$]
$NbOPO_4$	119	1.2	10.1	4.1
Nb_2O_5	115	0.5	4.3	1.6
TiO_2-PO_4	220	0.2	0.9	1.4

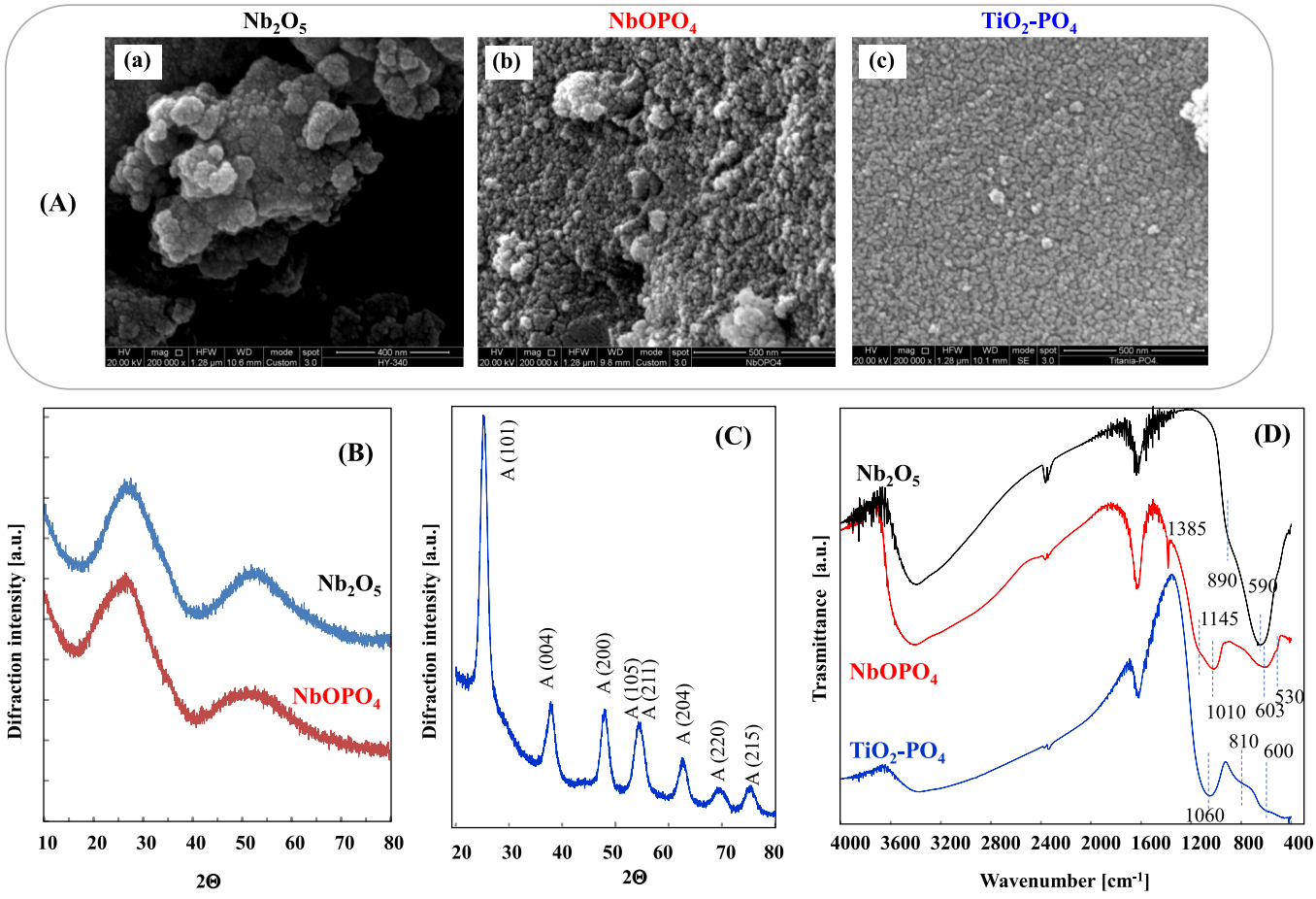

Fig. 2. (A) SEM microphotographs of (a) Nb_2O_5, (b) $NbOPO_4$ and (c) TiO_2-PO_4; XRD diffraction pattern of (B) Nb_2O_5 and $NbOPO_4$; (C) TiO_2-PO_4 and (D) FTIR of the three catalysts.

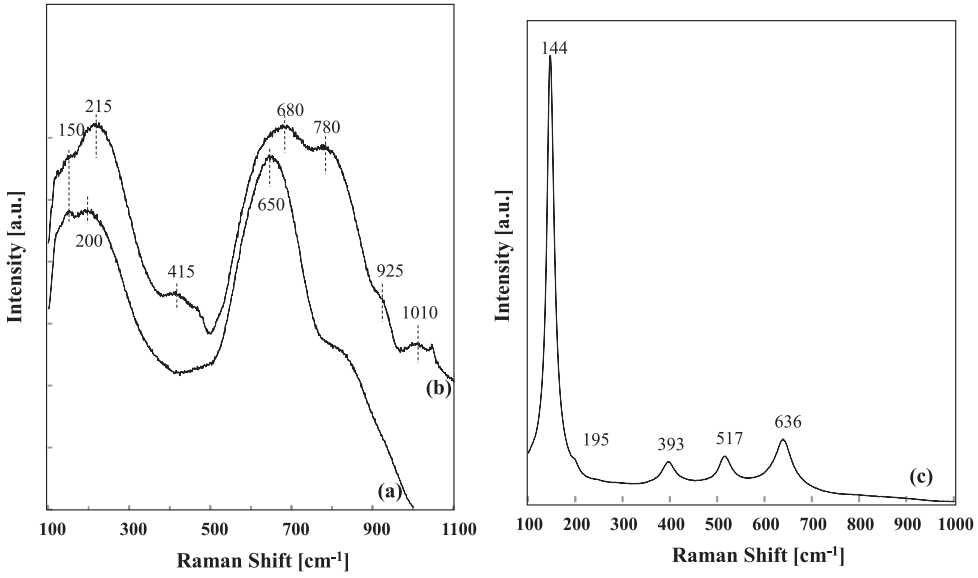

Fig. 3. Raman spectra of: (a) Nb_2O_5; (b) $NbOPO_4$ and (c) TiO_2-PO_4.

the thermal stability of the samples was, moreover, performed by thermogravimetric analysis (TGA) experiments using a TGA/DSC1 STAR Mettler Toledo Inc. apparatus. In particular, the samples (15 mg) were treated in N_2 flow (30 mL min^{-1}) from 25 °C to 1100 °C with a heating rate of 10 °C min^{-1}. For the NH_3-TPD test, before starting the ammonia adsorption experiment, the samples (c.a 200 mg) were pre-treated in He flow at 300 ∘C for 30 min, in order to clean the surface and desorb any water, according to TGA experiments. After cooling to room temperature, a stream of 5 % NH_3/He (30 mL min^{-1}) was flowed for 1 h until saturation. The samples were further purged in flowing He (100 mL min^{-1}) at 100 °C for 1 h to remove physically adsorbed ammonia, and then, cooled down to room temperature. Ammonia desorption was monitored with the above-mentioned ABB, UV gas analyser (the concentration of ammonia (ppm) was registered in the flow with the step of one second), under He flow (30 mL min^{-1}) heating up to 650 °C (rate of 10 °C min^{-1}), that is the temperature at which the ammonia was totally desorbed, then, the acquisition of data was stopped. Before the gas detection system, a cold trap was used to condense any water desorbed from the sample. The ammonia concentration profiles, ppm of NH_3 desorbed $g^{-1}s^{-1}$ under He flow were plotted versus time and temperature and the total amount of desorbed NH_3 [mmol NH_3 g^{-1}] was calculated by the integration of the curves.

2.3. OMW, OVP, DPP and DL valorization by heterogeneous catalytic process

The heterogeneous catalytic reactions were carried out in the presence of the commercial Nb_2O_5, $NbOPO_4$ or in house prepared phosphated titania. A stainless-steel autoclave (Tefic Biotech Co. Limited, Xi'an, China) with a 50 mL PTFE reaction chamber (hydrothermal reactor) was placed in a thermostatic, preheated synthetic oil bath, further located over a heated magnetic stirrer. The reactor was charged with 2 mL of pre-filtered OMW solution (as received or after liquid–liquid extraction of polyphenols), 22 mL of distilled water and with 80 mg of catalyst. For the solid waste fractions (OVP, DPP or DL), 40 mg of substrate either previously treated or untreated, together with 80 mg of $NbOPO_4$ and 24 mL of water were placed inside the reactor. Reactions were performed at 210 °C, at different reaction times under continuously stirring at 500 rpm. These experimental conditions were as those optimized in our previous study [21]. After the desired reaction time, the autoclave was cooled down up to room temperature (ca. 25 °C). The collected samples were then filtered through a 0.45 μm membrane filter (CA, Millipore) and the liquid injected into a Thermo Scientific Dionex Ultimate 3000 HPLC equipped with a diode array and refractive index detectors. The separation column was a REZEK ROA Organic acid H+Phenomenex and the eluent an aqueous 2.5 mM H_2SO_4 solution with a flow rate equal 600μL min^{-1}. The characteristic HPLC chromatogram showing the retention times of 5-HMF and furfural in a typical catalytic experiment is shown in Figure S4. Retention times and UV spectra of the compounds were compared with those of standards purchased from Sigma-Aldrich with a purity of > 99 %. The catalytic performance in terms of 5-HMF and furfural yields percentage (Y) was calculated as follows:

$$Y_{HMF} = \frac{[5-HMF]}{[\text{total hexoses}]} \bullet 100 \quad (1)$$

$$Y_F = \frac{[\text{furfural}]}{[\text{total pentoses}]} \bullet 100 \quad (2)$$

Where [5-HMF] and [furfural] are the concentration of these two species measured at the end of each catalytic experiment and [total hexoses] and [total pentoses] corresponds to the concentration of these species present in the reacting biomass measured by HPLC after the enzymatic hydrolysis.

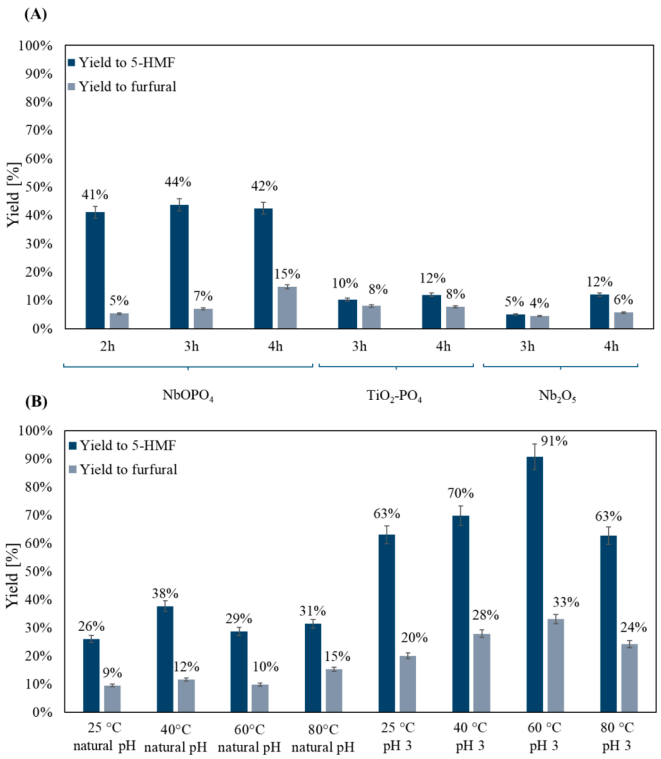

Fig. 4. Valorization of OMW to furans by heterogeneous catalytic process performed at 210 °C (A) in the presence of different catalysts and at different reaction times, (B) in the presence of $NbOPO_4$ catalyst (reaction time 3 h) on aqueous solution obtained after the separation of the polyphenols from the OMW carried out under different experimental conditions. Error bars indicate a standard deviation of ca. 5 %.

3. Results and discussion

3.1. Characterization of the olive oil biomass wastes

The total sugars analyzed by the Dubois methodology in the OMW before and after polyphenols extraction and in the solid wastes are reported in Table 1. The results indicate that after the separation of polyphenols, the aqueous solution contains about the same quantity of sugars, suggesting that the separation of the polyphenols did not interfere with the subsequent valorization of the carbohydrate content.

The polyphenol species (hydroxytyrosol, verbascoside and oleuropein) in the as received OMW and in the methanol solution after their liquid–liquid extraction with ethyl acetate, at different temperature and pH, did not significantly changed (Fig. 1), thus the recovery was very efficient. The OMW samples contained high concentration of hydroxytyrosol (up to 1300 ppm), in line with literature [22,23], which is a high value antioxidant and radical scavenger. The total content of verbascoside in the OMW was nearly 40 ppm while that of oleuropein was around 30 ppm. Consistent with the findings of other researchers [24], higher temperatures slightly enhanced the extraction efficiency while, the decrease of pH did not yield a significantly improvement in the extraction efficiency.

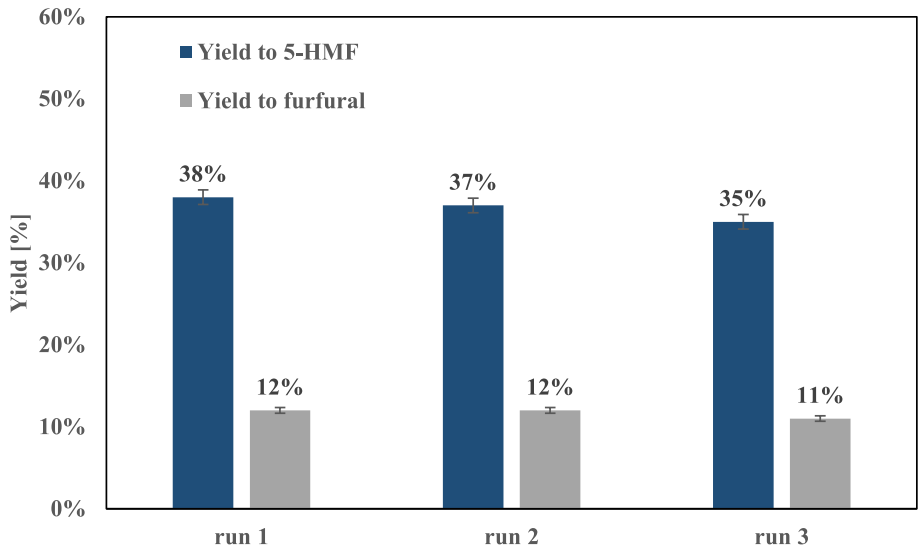

Fig. 5. $NbOPO_4$ stability tests performed with three consecutive runs (reaction time 3 h) using as the substrate the OMW aqueous solution obtained after polyphenols separation at 40 °C and at natural pH. Error bars indicate a standard deviation of ca. 5 %.

3.2. Catalysts characterization

The results of textural characterization of the Nb_2O_5, $NbOPO_4$ and TiO_2-PO_4 catalysts are shown in Table 2 and S1. Nb_2O_5 and $NbOPO_4$ catalysts presented similar specific surface areas (SSA). The N_2 adsorption–desorption isotherms (see Figures S5) of $NbOPO_4$ revealed pores with higher size and volume than Nb_2O_5 due to the characteristic 2-D lamellar structure of $NbOPO_4$ [21], even if both materials showed type IV isotherms [25]. The $NbOPO_4$ was characterized by a broad pore size distribution centered at around 10 nm, with a cumulative pore volume equal to 0.23 $cm^3 \cdot g^{-1}$, whereas Nb_2O_5 showed a narrower pore distribution centered at around 5 nm with a pore volume of 0.13 $cm^3 \cdot g^{-1}$. The SSA of TiO_2-PO_4 sample was approximately double than the other two catalysts, with a relatively high pore volume (0.19 $cm^3 \cdot g^{-1}$) and the corresponding mean pore size was centered at around 3 nm. The preparation procedure of the TiO_2-PO_4 in the presence of triblock copolymer confers a mesoporous framework to this material [26].

The nanostructure of Nb_2O_5, $NbOPO_4$ and TiO_2-PO_4 materials shown in the SEM pictures (Fig. 2A), included nanoparticles agglomerates ranging from 20-40 nm, 12–20 nm and 19–30 nm, respectively. The elemental composition and distribution of the catalysts revealed by EDX (Table S2) showed the homogenous distribution and stoichiometric amount of Nb, O and P in the Nb_2O_5 and $NbOPO_4$. However, the homogenous distribution of Ti and P in the TiO_2-PO_4 catalyst measured by EDX (1:0.11), did not correspond to the nominal atomic ratio (1:0.05). This difference could be due to the superficial enrichment of titania with PO_4 groups, schematically shown in Figure S3. The chemical-physical characterization of the two commercial CBMM catalysts is reported in earlier studies, and the present results confirm the features already published [25,27–32]. The elemental composition and distribution of the catalysts by XPS (see Figures S6-S8) are reported in Table S2. The results for Nb_2O_5 are consistent with a higher presence of coordinatively unsaturated Lewis acid sites in the surface layers (lower relative oxygen content). Conversely, $NbOPO_4$ and TiO_2-PO_4 presented P enrichment on the top of their surface, which was particularly higher in the phosphated titania (in accordance with the results obtained by EDX analysis that however is a semi-bulk analytical technique) in comparison to the nominal value.

The XRD patterns (Fig. 2B) showed the amorphous nature of both Nb-based materials. They mainly exhibited two broad peaks at 2θ equal ca. 25° and 52°, confirming the amorphous features in agreement with previous studies [33–37]. Conversely, the phosphated titania exhibited the typical anatase diffraction peaks of TiO_2 (Fig. 2 (C)) as previously shown [38].

The FTIR spectra of the solids, reported in Fig. 2D, showed very broad bands centered at around 3400 and 1620 cm^{-1} corresponding to the surface-adsorbed water and hydroxyl groups [39]. The wide band centered at 3400 cm^{-1} corresponds to the –OH vibration of physiosorbed H_2O molecules as well as to the stretching vibrations of the Nb-OH or Ti-OH species. The stretching vibration of the P-OH bond, which would appear at ca. 3030 cm^{-1}, are hardly visible. The transition at 1620 cm^{-1} is attributed to the bending vibration of water molecules. The signals in the range 400–1200 cm^{-1} are characteristic transitions of the oxide lattice in Nb_2O_5 and TiO_2 matrix, particularly Nb-O-Nb [40] and Ti-O-Ti. The IR absorption large band centered at ca. 810 and 600 cm^{-1} can be attributed to the Ti-O vibrations in the TiO_2 as well as the bending of P-O-H group [38,41]. The wide transition between 1200 and 900 cm^{-1} is attributed to the stretching modes of P-O bonds. A broad transition centered at 1060 cm^{-1} is assigned to PO_4^{3-} [41], however, the absence of the band corresponding to the stretching attributed to P=O, located at ca. 1300 cm^{-1}, suggested that the quantity of PO_4^{3-} species on the surface of TiO_2-PO_4 catalyst was below the detection limit. On the opposite, this transition was revealed at 1385 $cm^{-1}$for $NbOPO_4$.

The Raman spectra (Fig. 3) of Nb_2O_5 shows two broad vibrational transitions centered at ca. 660 and 200 cm^{-1}. The structure of the Nb_2O_5 consists of distorted NbO_6, NbO_7 and NbO_8 polyhedra containing also water molecules bonded by hydrogen bonds to the oxygens of various strengths. These hydrated polyedra are responsible for the Brønsted acid centers. The band at ca. 600 cm^{-1} is attributed to the stretching vibrations of the Nb-O-Nb bridging bond of distorted octahedral. The weak and broad transition centered at ca. 200 cm^{-1} has been assigned to the

bending modes of the Nb-O-Nb linkages [42]. The Raman spectrum of $NbOPO_4$ is characterized by the strong transition at 680 cm^{-1}, assigned to the stretching O-Nb-O mode of the distorted NbO_6 polyhedra and by the presence of the phosphate units. The phosphates vibrational transitions are responsible for the group of bands in the range 750 to 1100 cm^{-1}. For instance, the signal at 780 cm^{-1} can be attributed to stretching P-O-P but also to O-Nb-O bonds coupled to O-P-O deformation modes; and the shoulder centered at ca. 925 and 1010 cm^{-1} to the O-P-O the symmetric and asymmetric stretching, respectively. The Raman spectrum of the TiO_2-PO_4 specimen, in agreement with the results of XRD investigation, shows only the characteristic signals corresponding to the pure anatase polymorph, with the signals centered at 144, 195, 393, 517, and 636 cm^{-1} attributable to the Eg, Eg, B1g, A1g and B2g modes of anatase TiO_2 [43].

The acidity of the three catalysts in aqueous suspension was determined by titration with NaOH. This method quantifies only the Brønsted acid sites through the measurement of free protons in solution due to the initial cation exchange between the catalyst surface and the solvent. The acidity measured by titration (Table 2) evidenced the much higher acidity of $NbOPO_4$ compared to Nb_2O_5 and TiO_2-PO_4, which resulted the least acid catalyst. However, literature reports that materials prepared in analogous manner exhibits Ti ions in tetrahedral coordination acting as Lewis acidic sites [38].

The thermal stability of the catalysts was determined by TGA (Figure S9). TiO_2-PO_4, Nb_2O_5 and $NbOPO_4$ showed a mass loss of about 11 %, 15 % and 17 %, respectively in the low-temperature range up to 300 °C that is most likely attributed to the release of water (Figure S9), indicating the hydrated state of these catalysts. The acidity of the materials and the amount and the strength of both Brønsted and Lewis acid sites of the catalysts were studied also by NH_3-TPD [29]. Figure S10 displays the NH_3 desorption under helium flow as a function of the temperature from ca. 50 up to 650 °C. Table 2 lists the acidity values derived from the NH_3-TPD study in terms of the total amount of desorbed NH_3 per gram of catalyst [mmol NH_3 g^{-1}]. Broad peaks covering almost the entire range of temperature, 200–600 °C, with an area corresponding to 1.6 and 1.4 mmol NH_3 g^{-1}, respectively, characterized the NH_3-TPD profiles of Nb_2O_5 and TiO_2-PO_4. The curves, being centred at around 300 and 255 °C, suggest the presence of weak and medium acid sites, in both samples [29]. The contribution of some strong acid sites was also detected in the Nb_2O_5 showing a further peak at 460 °C. The most acidic sample was the $NbOPO_4$ characterized by an intense peak centred at around 400 °C with a total acidity of 4.1 mmol NH_3 g^{-1}. The shape of the curve and desorption temperature suggest mainly the presence of strong acidic sites. These results are in agreement with those obtained by the titration method but indicate moreover that the acid sites of the $NbOPO_4$ are also stronger with respect to those of the other two catalysts.

3.3. Heterogeneous catalytic OMW valorization

The catalytic valorization of OMW in terms of furans (5-HMF and furfural) yields before and after polyphenols extraction is shown in Fig. 4. $NbOPO_4$ provided the highest yields of 5-HMF up to 44 %, while the yields of 5-HMF with TiO_2-PO_4 and Nb_2O_5 were only about 12 % in the best cases. The yield of furfural was lower (Fig. 4A), possibly due to the low fraction of arabinose monomer (Table S3) in the original OMW matrix. The yield to 5-HMF with $NbOPO_4$ showed insignificant change between 2–4 h of reaction time, although the yield was expected to decrease at longer reaction times as a result of its transformation to side products (Figure S2) [29]. Similarly, this last behavior was observed also with TiO_2-PO_4. On the contrary, the yield of 5-HMF in the presence of Nb_2O_5 increased with reaction time. This insight could be attributed to the lower specific surface area and acidity of Nb_2O_5 (Table 2) resulting in longer reaction times to be effective. In fact, Nb_2O_5 presents both LAS and BAS, where LAS are able to isomerise glucose into fructose [32], and BAS are active for the dehydration of fructose to 5-HMF. An excess of LAS may have a deleterious effect on the 5-HMF yield due to the formation of by-products [44], as shown in Figure S2. Since, Nb_2O_5 possesses a lower number of BAS compared to $NbOPO_4$ a lower catalytic performance was expected (Fig. 4A). Although the TiO_2-PO_4 catalyst has lower acidity than Nb_2O_5, the yield of 5-HMF was similarly to Nb_2O_5 due to its higher SSA. The much lower yield to furfural increased with reaction time with $NbOPO_4$ and remained approximately unchanged with the other two catalysts.

It is interesting to note that the only species detected in solution during the catalytic tests were 5-HMF and furfural and sugars deriving from OMW which were not totally converted. Consequently, the obtained solution after the reaction was not pure in furans, but this problem may be easily overcome by employing selective organic solvents, such as methyl isobutyl ketone, for the separation of the products. On the other hand, the formation of solid humins were always observed even if their quantification was very difficult.

The results obtained after 3 h of reaction with the most active $NbOPO_4$ catalyst and after the extraction of polyphenols from the water matrix are shown in Fig. 4B. The results with the sample extracted at natural pH were comparable to those obtained with the as received OMW. In sharp contrast, the yield of furans with the sample extracted at acidic pH were significantly higher. This yield increase was attributed to the residual HCl in the water phase left after the polyphenols extraction process, thus the combined catalytic action of the heterogeneous ($NbOPO_4$) and homogeneous (HCl) catalysts increased the conversion of sugars to furans. While HCl is a well-known effective homogeneous catalyst, its use raises concerns related to its sustainability, safety, and disposal. Consequently, its utilization does not align with the objectives of this study. The results obtained suggest that OMW can be valorized in a more sustainable way through a two-step process, involving biphasic extraction of polyphenols followed by a heterogeneous chemical reaction. The extraction at natural pH is the greenest option although the yield to furans was lower than at pH 3. While various catalytic processes for the treatment and valorization of OMW have been documented in the literature, this study marks the pioneering use of a double recovery process. This innovative approach offers economic advantages in the production of fine chemicals.

Finally, the stability of the $NbOPO_4$ catalyst was evaluated in three consecutive runs using the OMW substrate after the polyphenols were removed at 40 °C under natural pH (Fig. 4B). After each catalytic run the catalyst was separated from the reacted solution by centrifugation and washed three times with hot water to clean its surface and reused. Fig. 5 shows a very good stability of the $NbOPO_4$ catalyst, with the yield of both 5-HMF and furfural decreasing of approximately 8 % after the third run, although this could be attributed to the loss of small quantities of catalyst during the washing process.

3.4. Valorization of the solid waste fractions: OVP, DPP and DL

The conversion of sugars, present in the solids waste fractions, to furans was investigated using $NbOPO_4$, which was identified as the most active catalyst. In contrast to the results obtained with OMW, the yield to furfural (Fig. 6) from all the three solid fractions was significantly higher and in general higher also than the yield to 5-HMF. This is due to the different composition of the solids' matrices compared to that of OMW. In fact, olive virgin pomace contains mainly cellulose, hemicellulose and lignin [45], while hemicellulose is a well-known component of the olive leaves [46].

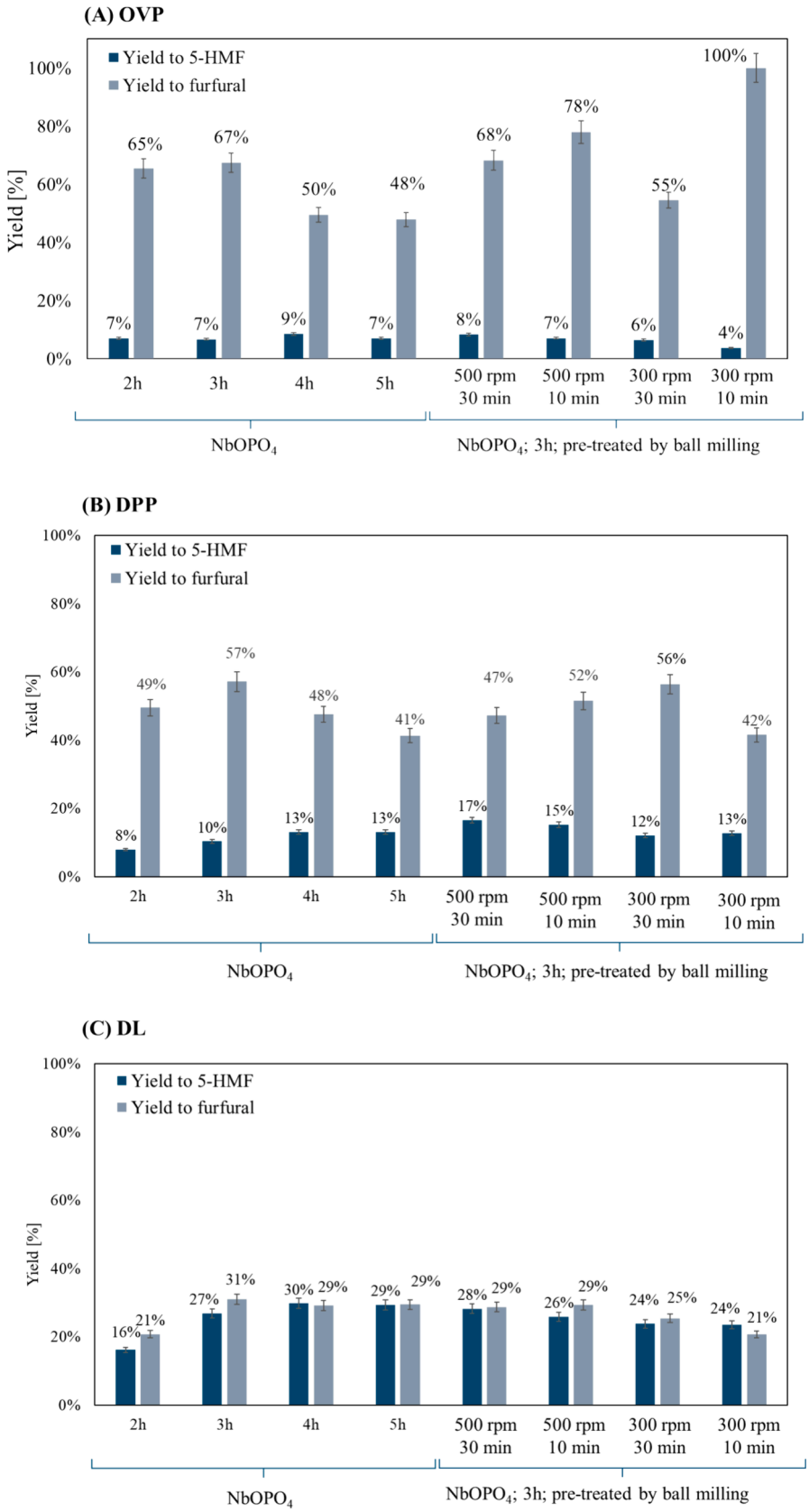

Fig. 6. Valorization of OVP, DPP, DL to furans by employing heterogeneous catalytic process with and without pre-treatment of the matrix. (A) OVP, (B) DPP, (C) DL. For all the runs, 40 mg of substrate either previously treated or untreated, along with 80 mg of solid catalyst and 24 mL of water were placed in the reactor and catalytically treated at 210 °C.

Hemicellulose contains mainly pentose sugars such as xylose [47] which yield furfural better then arabinose whose presence was instead observed in the OMW (see Table S3). The superior yield to furfural from xylose than from arabinose has also been observed [48,49].

The catalytic reactions were carried out both with and without a ball milling pre-treatment at different rotations per minute (rpm) and times. Without such pre-treatment, 3 h reaction time on the OVP and DPP fractions returned the highest yields of furfural (67 % for OVP and 57 % for DPP), while the yields to 5-HMF were less significant. Conversely, the yields to 5-HMF and furfural with the DL fraction was approximately the same (about 30 %) with an optimum reaction time of about 3–5 h.

The reaction with ball milled substrate after 3 h of reaction time did not improve the yield of furans with the DPP and DL solid fractions, most likely due to the hardness of these substrates. However, it had a positive influence, in some tests, on the treatment of OVP that gave higher furfural yield particularly for shorter pre-treatment time (300 or 500 rpm for 10 min). In the best cases, the yield to furfural increased up to 78 % (500 rpm, 10 min) or up to 100 % (300 rpm, 10 min). This probably occurred since a brief treatment is able to reduce the particle size of the solid waste enhancing the yields to furans, whereas the high temperatures generated locally inside the jar of the ball milling apparatus after longer treatment times could result in the partial combustion of the sugar molecules to be catalytically transformed to furans.

4. Conclusion

This study has demonstrated the production of furans, 5-HMF and furfural, from the valorization of olive mill biomass waste fractions using Nb_2O_5, $NbOPO_4$ and TiO_2-PO_4 heterogeneous catalysts. Overall, the use of such heterogenous catalysts increases the sustainability and green credentials of the valorization process in comparison to the use of homogeneous catalysts. $NbOPO_4$ was the most active catalyst due to its higher acidity. The yield of 5-HMF (the predominant furan species observed) from the OMW fraction with this catalyst only slightly decreased (from 44 % to 38 %) after polyphenols extraction at natural pH. Thus, the OMW can be effectively valorized through a two-step process, involving biphasic extraction of polyphenols followed by a heterogeneous chemical reaction, avoiding the use of homogenous acids. The catalytic valorization of the solid wastes OVP, DPP and DL over $NbOPO_4$ produced predominantly furfural with a yield of 100 % from OVP and 57 % from DPP. On the contrary, the treatment of DL, gave rise similar yields (ca. 30 %) for both furfural and 5-HMF. Overall, this study holds significant relevance due to its novel approach with significant potential for the valorization of agricultural waste. This novel perspective aligns well with the principles of circular economy, reducing waste generation by its conversion to valuable products.

CRediT authorship contribution statement

Serena Lima: Writing – review & editing, Writing – original draft, Visualization, Validation, Supervision, Software, Resources, Methodology, Investigation, Funding acquisition, Formal analysis, Data curation, Conceptualization. **Tea Ricotta:** Methodology, Investigation. **Elisa I. García-López:** Writting, Review and editing, Writting original draft, Validation, Supervision, Methodology, Investifgation, Formal analysis, Data curation, Conceptualization. **Leonarda F. Liotta:** Investigation, Validation, Data curation, Writting review and editing. **Silvia Villar-Rodil:** Investigation, Validation, Writing – review & editing. **Gianluca Li Puma:** Writing – review & editing, Writing – original draft, Validation, Supervision, Methodology, Formal analysis, Data curation, Conceptualization. **Giuseppe Marcì:** Writing – review & editing, Writing – original draft, Visualization, Validation, Supervision, Resources, Methodology, Investigation, Funding acquisition, Formal analysis, Data curation, Conceptualization. **Francesca Scargiali:** Writting, Review and editing, Writting original draft, Validation, Supervision, Methodology, Investifgation, Formal analysis, Data curation, Conceptualization, Funding adquisition.

Declaration of competing interest

The authors declare that they have no known competing financial interests or personal relationships that could have appeared to influence the work reported in this paper.

Data availability

Data will be made available on request.

Acknowledgements

Part of this work was carried out with the co-funding of European Union, European Social Fund – REACT EU, *PON Ricerca e Innovazione 2014-2020, Azione IV.6 "Contratti di ricerca su tematiche Green" (DM 1062/2021)*.

Authors wish to thank Aten Center for the analysis on polyphenolic content of OMW and the Azienda Agricola D'Anna Francesca for providing the samples.

Appendix A. Supplementary data

Supplementary data to this article can be found online at https://doi.org/10.1016/j.cej.2024.154654.

References

[1] C.O. Tuck, E. Pérez, I.T. Horváth, R.A. Sheldon, M. Poliakoff, Valorization of Biomass: Deriving More Value from Waste, Science 337 (2012) 695–699, https://doi.org/10.1126/science.1218930.
[2] S. Dermeche, M. Nadour, C. Larroche, F. Moulti-Mati, P. Michaud, Olive mill wastes: Biochemical characterizations and valorization strategies, Process Biochem. 48 (2013) 1532–1552, https://doi.org/10.1016/j.procbio.2013.07.010.
[3] P.S. Rodis, V.T. Karathanos, A. Mantzavinou, Partitioning of Olive Oil Antioxidants between Oil and Water Phases, J. Agric. Food Chem. 50 (2002) 596–601, https://doi.org/10.1021/jf010864j.
[4] M.J. Negro, P. Manzanares, E. Ruiz, E. Castro, M. Ballesteros, The biorefinery concept for the industrial valorization of residues from olive oil industry, Olive Mill Waste. Elsevier, in, 2017, pp. 57–78.
[5] T. Miranda, J.I. Arranz, I. Montero, S. Román, C.V. Rojas, S. Nogales, Characterization and combustion of olive pomace and forest residue pellets, Fuel Process. Technol. 103 (2012) 91–96, https://doi.org/10.1016/j.fuproc.2011.10.016.
[6] A.R. Tekin, A.C. Dalgıç, Biogas production from olive pomace, Resour. Conserv. Recycl. 30 (2000) 301–313, https://doi.org/10.1016/S0921-3449(00)00067-7.
[7] M. Ayadi, S. Awad, A. Villot, M. Abderrabba, M. Tazerout, Heterogeneous acid catalyst preparation from olive pomace and its use for olive pomace oil esterification, Renew. Energy 165 (2021) 1–13, https://doi.org/10.1016/j.renene.2020.11.031.
[8] Y. Rharrabti, M.E.I. Yamani, Olive Mill Wastewater: Treatment and Valorization Technologies, in: Handbook of Environmental Materials Management, Springer International Publishing, Cham, 2018, pp. 1–28, https://doi.org/10.1007/978-3-319-58538-3_91-1.
[9] P. Paraskeva, E. Diamadopoulos, Technologies for olive mill wastewater (OMW) treatment: a review, J. Chem. Technol. Biotechnol. 81 (2006) 1475–1485, https://doi.org/10.1002/jctb.1553.
[10] D. Montané, High-temperature dilute-acid hydrolysis of olive stones for furfural production, Biomass and Bioenergy 22 (2002) 295–304, https://doi.org/10.1016/S0961-9534(02)00007-7.
[11] D. Soukup-Carne, X. Fan, J. Esteban, An overview and analysis of the thermodynamic and kinetic models used in the production of 5-hydroxymethyl-furfural and furfural, Chem. Eng. J. 442 (2022) 136313, https://doi.org/10.1016/j.cej.2022.136313.
[12] A.A. Rosatella, S.P. Simeonov, R.F.M. Frade, C.A.M. Afonso, 5-Hydroxymethylfurfural (HMF) as a building block platform: Biological properties, synthesis and synthetic applications, Green Chem. 13 (2011) 754, https://doi.org/10.1039/c0gc00401d.
[13] Y. Román-Leshkov, C.J. Barrett, Z.Y. Liu, J.A. Dumesic, Production of dimethylfuran for liquid fuels from biomass-derived carbohydrates, Nature 447 (2007) 982–985, https://doi.org/10.1038/nature05923.
[14] S. Singhal, S. Agarwal, M.P. Mudoi, N. Singhal, R. Singh, Chemical conversion of furan dicarboxylic acid to environmentally benign polyesters: an overview, Biomass Convers. Biorefinery 13 (2023) 15619–15636, https://doi.org/10.1007/s13399-021-01871-6.

[15] M.I. Badawy, F.E. Gohary, M.Y. Ghaly, M.E.M. Ali, Enhancement of olive mill wastewater biodegradation by homogeneous and heterogeneous photocatalytic oxidation, J. Hazard. Mater. 169 (2009) 673–679, https://doi.org/10.1016/j.jhazmat.2009.04.038.
[16] S. De Rosa, G. Giordano, T. Granato, A. Katovic, A. Siciliano, F. Tripicchio, Chemical pretreatment of olive oil mill wastewater using a metal-organic framework catalyst, J. Agric. Food Chem. 53 (2005) 8306–8309, https://doi.org/10.1021/jf0512609.
[17] I. Nowak, M. Ziolek, Niobium Compounds: Preparation, Characterization, and Application in Heterogeneous Catalysis, Chem. Rev. 99 (1999) 3603–3624, https://doi.org/10.1021/cr9800208.
[18] M. DuBois, K.A. Gilles, J.K. Hamilton, P.A. Rebers, F. Smith, Colorimetric Method for Determination of Sugars and Related Substances, Anal. Chem. 28 (1956) 350–356, https://doi.org/10.1021/ac60111a017.
[19] P. Carniti, A. Gervasini, F. Bossola, V. Dal Santo, Cooperative action of Brønsted and Lewis acid sites of niobium phosphate catalysts for cellobiose conversion in water, Appl. Catal. B Environ. 193 (2016) 93–102, https://doi.org/10.1016/j.apcatb.2016.04.012.
[20] L.M. Yang, Y.J. Wang, G.S. Luo, Y.Y. Dai, Functionalization of SBA-15 mesoporous silica with thiol or sulfonic acid groups under the crystallization conditions, Microporous Mesoporous Mater. 84 (2005) 275–282, https://doi.org/10.1016/j.micromeso.2005.05.037.
[21] S. Lima, E.I. García-López, A. Adawy, G. Marcì, F. Scargiali, Valorisation of Chlorella sp. biomass in 5-HMF through a two-step conversion in the presence of Nb_2O_5 and $NbOPO_4$ and optimisation through reactive extraction, Chem. Eng. J. 471 (2023) 144583, https://doi.org/10.1016/j.cej.2023.144583.
[22] N. Allouche, I. Fki, S. Sayadi, Toward a High Yield Recovery of Antioxidants and Purified Hydroxytyrosol from Olive Mill Wastewaters, J. Agric. Food Chem. 52 (2004) 267–273, https://doi.org/10.1021/jf034944u.
[23] M. Russo, I.L. Bonaccorsi, F. Cacciola, L. Dugo, L. De Gara, P. Dugo, L. Mondello, Distribution of bioactives in entire mill chain from the drupe to the oil and wastes, Nat. Prod. Res. 35 (2021) 4182–4187, https://doi.org/10.1080/14786419.2020.1752208.
[24] A. Antony, M. Farid, Effect of Temperatures on Polyphenols during Extraction, Appl. Sci. 12 (2022) 2107, https://doi.org/10.3390/app12042107.
[25] P. Carniti, A. Gervasini, S. Biella, A. Auroux, Niobic acid and niobium phosphate as highly acidic viable catalysts in aqueous medium: Fructose dehydration reaction, Catal. Today 118 (2006) 373–378, https://doi.org/10.1016/j.cattod.2006.07.024.
[26] K. Hadjiivanov, Study of phosphate-modified TiO_2 (anatase), J. Catal. 116 (1989) 498–505, https://doi.org/10.1016/0021-9517(89)90116-4.
[27] P.M. De Souza, L.A. De Sousa, F.B. Noronha, R. Wojcieszak, Dehydration of levoglucosan to levoglucosenone over solid acid catalysts. Tuning the product distribution by changing the acid properties of the catalysts, Mol. Catal. 529 (2022) 112564, https://doi.org/10.1016/j.mcat.2022.112564.
[28] M.M.J. Junior, S.A. Fernandes, E. Borges, B.E.L. Baêta, F.A. Rodrigues, Kinetic study of the conversion of glucose to 5-hydroxymethylfurfural using niobium phosphate, Mol. Catal. 518 (2022) 112079, https://doi.org/10.1016/j.mcat.2021.112079.
[29] S. Lima, E.I. García-López, I. Krivtsov, M. Ilkaeva, C. Bornes, L. Mafra, L.F. Liotta, S. Villar-Rodil, J.I. Paredes, G. Marcì, F. Scargiali, Valorisation of microalga Chlorella sp. into furans in the presence of Nb_2O_5 catalysts, J. Catal. 433 (2024) 115457, https://doi.org/10.1016/j.jcat.2024.115457.
[30] J.A. Santana, W.S. Carvalho, C.H. Ataíde, Catalytic effect of ZSM-5 zeolite and HY-340 niobic acid on the pyrolysis of industrial kraft lignins, Ind. Crops Prod. 111 (2018) 126–132, https://doi.org/10.1016/j.indcrop.2017.10.023.
[31] K.M.A. Santos, E.M. Albuquerque, L.E.P. Borges, M.A. Fraga, Discussing Lewis and Brønsted acidity on continuous pyruvaldehyde Cannizzaro reaction to lactic acid over solid catalysts, Mol. Catal. 458 (2018) 198–205, https://doi.org/10.1016/j.mcat.2017.12.010.
[32] J.L. Vieira, G. Paul, G.D. Iga, N.M. Cabral, J.M.C. Bueno, C. Bisio, J.M.R. Gallo, Niobium phosphates as bifunctional catalysts for the conversion of biomass-derived monosaccharides, Appl. Catal. A Gen. 617 (2021) 118099, https://doi.org/10.1016/j.apcata.2021.118099.
[33] M.N. Catrinck, E.S. Ribeiro, R.S. Monteiro, R.M. Ribas, M.H.P. Barbosa, R. F. Teófilo, Direct conversion of glucose to 5-hydroxymethylfurfural using a mixture of niobic acid and niobium phosphate as a solid acid catalyst, Fuel 210 (2017) 67–74, https://doi.org/10.1016/j.fuel.2017.08.035.
[34] Y. Ma, J. Wang, W. Tan, J. Jiang, J. Xu, K. Wang, Directional liquefaction of lignocellulosic biomass for value added monosaccharides and aromatic compounds, Ind. Crops Prod. 135 (2019) 251–259, https://doi.org/10.1016/j.indcrop.2019.04.038.
[35] Q. Sun, Y. Fu, H. Yang, A. Auroux, J. Shen, Dehydration of methanol to dimethyl ether over Nb_2O_5 and $NbOPO_4$ catalysts: Microcalorimetric and FT-IR studies, J. Mol. Catal. A Chem. 275 (2007) 183–193, https://doi.org/10.1016/j.molcata.2007.06.008.
[36] P. Yang, D. Zhao, D.I. Margolese, B.F. Chmelka, G.D. Stucky, Block Copolymer Templating Syntheses of Mesoporous Metal Oxides with Large Ordering Lengths and Semicrystalline Framework, Chem. Mater. 11 (1999) 2813–2826, https://doi.org/10.1021/cm990185c.
[37] Y. Zhang, J. Wang, J. Ren, X. Liu, X. Li, Y. Xia, G. Lu, Y. Wang, Mesoporous niobium phosphate: an excellent solid acid for the dehydration of fructose to 5-hydroxymethylfurfural in water, Catal. Sci. Technol. 2 (2012) 2485, https://doi.org/10.1039/c2cy20204b.
[38] W. Guo, T. Kortenbach, W. Qi, E. Hensen, H. Jan Heeres, J. Yue, Selective tandem catalysis for the synthesis of 5-hydroxymethylfurfural from glucose over in-situ phosphated titania catalysts: Insights into structure, bi-functionality and performance in flow microreactors, Appl. Catal. B Environ. 301 (2022) 120800, https://doi.org/10.1016/j.apcatb.2021.120800.
[39] K. Nakamoto, Infrared and Raman spectra of inorganic and coordination compounds, 4th ed., Wiley, New York, 1986.
[40] L.J. Burcham, J. Datka, I.E. Wachs, In Situ Vibrational Spectroscopy Studies of Supported Niobium Oxide Catalysts, J. Phys. Chem. B 103 (1999) 6015–6024, https://doi.org/10.1021/jp990289a.
[41] A. Bhaumik, S. Inagaki, Mesoporous Titanium Phosphate Molecular Sieves with Ion-Exchange Capacity, J. Am. Chem. Soc. 123 (2001) 691–696, https://doi.org/10.1021/ja002481s.
[42] Y. Repelin, E. Husson, F. Bennani, C. Proust, Raman spectroscopy of lithium niobate and lithium tantalate. Force field calculations, J. Phys. Chem. Solids 60 (1999) 819–825, https://doi.org/10.1016/S0022-3697(98)00333-3.
[43] G. Busca, G. Ramis, J.M.G. Amores, V.S. Escribano, P. Piaggio, FT Raman and FTIR studies of titanias and metatitanate powders, J. Chem. Soc. Faraday Trans. 90 (1994) 3181, https://doi.org/10.1039/ft9949003181.
[44] E.I. García-López, F.R. Pomilla, B. Megna, B., M.L. Testa, L.F. Liotta, G. Marcì, Catalytic dehydration of fructose to 5-hydroxymethylfurfural in aqueous medium over Nb_2O_5-based catalysts. Nanomaterials 11 (2021). https://doi.org/10.3390/nano11071821.
[45] W. Han, Y. Geng, Optimization and characterization of cellulose extraction from olive pomace, Cellulose 30 (2023) 4889–4903, https://doi.org/10.1007/s10570-023-05195-8.
[46] A. Ben Mabrouk, J.L. Putaux, S. Boufi, Valorization of olive leaf waste as a new source of fractions containing cellulose nanomaterials, Ind. Crops Prod. 202 (2023) 116996, https://doi.org/10.1016/j.indcrop.2023.116996.
[47] A. Bercier, R. Plantier-Royon, C. Portella, Convenient conversion of wheat hemicelluloses pentoses (d-xylose and l-arabinose) into a common intermediate, Carbohydr. Res. 342 (2007) 2450–2455, https://doi.org/10.1016/j.carres.2007.07.010.
[48] B. Danon, W. Hongsiri, L. van der Aa, W. de Jong, Kinetic study on homogeneously catalyzed xylose dehydration to furfural in the presence of arabinose and glucose, Biomass and Bioenergy 66 (2014) 364–370, https://doi.org/10.1016/j.biombioe.2014.04.007.
[49] W. Hongsiri, B. Danon, W.de Jong, The effects of combined catalysis of oxalic acid and seawater on the kinetics of xylose and arabinose dehydration to furfural. Int. J. Energy Environ. Eng. 6 (2015) 21-30. https://doi.org/10.1007/s40095-014-0146-9.